View metadata, citation and similar papers at core.ac.uk

brought to you by CORE

provided by epublications@Marquette

Marquette University
e-Publications@Marquette

Electrical and Computer Engineering Faculty Research and Publications

Electrical and Computer Engineering, Department of

6-23-2014

Terahertz Photoacoustic Spectroscopy Using an MEMS Cantilever Sensor

Nathan E. Giauvitz
Air Force Institute of Technology

Ronald A. Coutu Jr.
Marquette University, ronald.coutu@marquette.edu

Ivan R. Medvedev
Wright State University

Douglas T. Petkie
Wright State University

Accepted version. *Journal of Microelectromechanical Systems,* Vol. 24, No. 1 (February 2015): 218-223. DOI. © 2015 IEEE. Used with permission.
Ronald A. Coutu was affiliated with the Air Force Institute of Technology, Wright-Patterson Airforce Base, OH at the time of publication.

Marquette University

e-Publications@Marquette

Electrical and Computer Engineering Faculty Research and Publications/College of Engineering

***This paper is NOT THE PUBLISHED VERSION;* but the author's final, peer-reviewed manuscript.** The published version may be accessed by following the link in the citation below.

Journal of Microelectromechanical Systems, Vol. 24, No. 1, (June, 2014): 216-223. DOI. This article is © Institute of Electrical and Electronic Engineers (IEEE) and permission has been granted for this version to appear in e-Publications@Marquette. IEEE does not grant permission for this article to be further copied/distributed or hosted elsewhere without the express permission from IEEE.

Contents

Abstract: 2
SECTION I. Introduction 2
A. THz Photoacoustic Spectroscopy 3
B. Cantilever Vibration Modeling 4
C. Fabrication and Experimental Setup 5
D. Results and Analysis 6
SECTION II. Conclusions 12
ACKNOWLEDGEMENTS 12
References 12

Terahertz Photoacoustic Spectroscopy Using an MEMS Cantilever Sensor

Nathan E. Glauvitz
Air Force Institute of Technology, Wright-Patterson Airforce Base, OH
Ronald A. Coutu
Air Force Institute of Technology, Wright-Patterson Airforce Base, OH
Ivan R. Medvedev
Wright State University, Dayton, OH
Douglas T. Petkie
Wright State University, Dayton, OH

Abstract:

In this paper, a microelectromechanical systems cantilever sensor was designed, modeled, and fabricated to measure the photoacoustic (PA) response of gases under very low vacuum conditions. The micromachined devices were fabricated using silicon-on-insulator wafers and then tested in a custom-built, miniature, vacuum chamber during this first-ever demonstration. Terahertz radiation was amplitude modulated to excite the gas under test and perform PA molecular spectroscopy. Experimental data show a predominantly linear response that directly correlates measured cantilever deflection to PA signals. Excellent low pressure (i.e., 2-40 mTorr) methyl cyanide PA spectral data were collected resulting in a system sensitivity of $1.97 \times 10^{-5}\ \mathrm{cm}^{-1}$ and a normalized noise equivalent absorption coefficient of $1.39 \times 10^{-9}\ \mathrm{cm}^{-1}\ \mathrm{W\,Hz}^{-1/2}$.

SECTION I. Introduction

Chemical sensing and spectroscopic detection can be accomplished using a variety of methods. In this work, a microelectromechanical system (MEMS) cantilever was used to directly measure the photoacoustic (PA) response of a gaseous agent excited by terahertz (THz) radiation. The PA effect was first published by Alexander Graham Bell in 1880 and has since been used to study solid, liquid and gas states of matter.[1] An advantage of PA spectroscopy, over traditional absorption spectroscopy, is that baseline measurements are not required.[2] Another major advantage is the reduced vacuum chamber size over traditional spectroscopy absorption cells that are typically 3-10 ft long.

Molecules can absorb and dissipate energy through different pathways such as electronic, radiative, vibrational, rotational or translational via collisions.[3,4] The PA effect results when molecules absorb energy from incident electromagnetic waves and then dissipate that energy through collisions and other non-radiative pathways. The resulting pressure variations or pressure waves can then be sensed using a microphone or some other pressure sensitive device.

In PA trace chemical detection and spectroscopy, there are several figures of merit (FOM) that are used to evaluate or compare system performance. For chemical detection systems, a species of interest is normally diluted with a non-absorbing gas and then the detection limit of the system is the minimum detectable concentration of the particular species. A high signal-to-noise ratio (SNR) is desirable because it determines the minimum absorption strength or system sensitivity ($\alpha_{\min}$)) given by

$$\alpha_{min} = \frac{\alpha_{peak}}{\mathrm{SNR}} \quad (1)$$

where α_{peak} is the strength of the measured absorption coefficient. Another useful FOM is the normalized noise equivalent absorption (NNEA) coefficient that is expressed as

$$\text{NNEA} = \alpha_{min} P_o \sqrt{T} \quad (2)$$

where P_o is the source power and T is the signal averaging time.[4] Fig. 1 above is a simulated absorption coefficient spectra for methyl cyanide (CH_3CN) at 18 mTorr of chamber pressure.

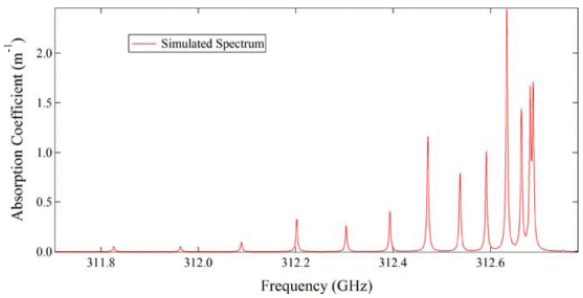

Fig. 1. Small region of the simulated absorption coefficient of methyl cyanide at 18 mTorr with applied pressure broadening conditions.

Several types of pressure sensors like tuning forks, membrane microphones, bridges and cantilevers have been used in THz and non-THz –based PA systems.[5–6,7,8,9,10,11,12,13,14,15,16,17,18,19,20] Non-THz–based PA systems are generally used to detect minimum concentrations of gases in nitrogen diluted environments. In these type of PA systems, relatively high chamber pressures ranging from 93-760 Torr are used resulting in NNEA's ranging from 1.4×10^{-9} to 1.8×10^{-9} cm^{-1} W $\text{Hz}^{-1/2}$. For THz -based PA systems, however, measurements must be collected at the lowest possible chamber pressure to ensure high spectral resolution. Krupnov and Burenin constructed a low pressure ($0.05 - 10$ Torr) spectrometer using a Mylar capacitive membrane microphone (3 μ m thick $\times$ 5 cm diameter) that resulted in minimum sensitivity data of 6×10^{-9} cm^{-1} .[9]

Categories for chamber pressure operating conditions are divided into three regions: intrinsic, molecular and viscous with each region named for its primary damping mechanism.[21] As previously discussed, non-THz PA systems operate at higher chamber pressures (93-760 Torr) where viscous damping dominates. The molecular regime is defined as the 7.5-750 mTorr range and the intrinsic regime is defined as pressure environments less than 7.5 mTorr.[21] A significant contribution of this work was using a MEMS cantilever sensor to collect high spectral resolution, low minimum sensitivity data in the lower molecular and upper intrinsic damping regimes (2-40 mTorr).

A. THz Photoacoustic Spectroscopy

When molecules are irradiated with THz, in low vacuum environments, they absorb energy in narrow quantized rotational states. The absorption frequency is a function of molecular structure, while absorption strength is dependent on both electric dipole moment and molecular structure. At low pressures, the dominant source of spectral line broadening is Doppler, due to the thermal motion of the absorbing atoms, and is represented mathematically as a Gaussian function. Pressure broadening, represented by a Lorentzian function, takes effect as pressures increases. In the THz spectral range the necessary low chamber pressures result in nearly equal Doppler and pressure broadening contributions.

To begin modeling THz PA performance, the energy absorbed during each THz radiation pulse (assuming a 50% duty cycle) is described as

$$\Delta E = \Delta P/(2f_m) \quad (3)$$

where ΔP is the power absorbed by the gas and f_{m} is the radiation source modulation frequency. The change in chamber pressure magnitude is then determined using the ideal gas law ($\Delta p = (N/V)k_B\Delta T$), the kinetic theory of gasses ($\Delta E = (3/2)Nk_B\Delta T$) and Beer's power absorption law given as

$$\Delta P = P_o - P = P_o p_x \alpha l \quad (4)$$

where P is the amount of unabsorbed power exiting the chamber, α is the absorption coefficient, p_x is the partial pressure of the gas under investigation and l is the chamber length. In this study, the partial pressure factor was set to one ($p_x = 1$) because no backfill gas was used to dilute the species and the volumetric fraction was only the gas under test. Using equations (3) and (4), the following equation for PA pressure change per cycle (Δp) was derived

$$\Delta p = \frac{P_o p_x \alpha l}{3Vf_m} = \frac{P_o \alpha}{3\pi r^2 f_m} \quad (5)$$

where V is the absorption chamber volume ($\pi\ r^2\ l$) and r is the radius of a cylindrical chamber.

Based on the design parameters in this study, the change in chamber pressure per cycle was expected to be approximately 18 μ Torr when using 0.1 mW of incident radiation source power. MEMS cantilevers, discussed next, was the key technology that enabled using a much smaller vacuum chamber ($2 \times 2 \times 2$ in 3) and very low chamber pressures during the PA spectral measurements.

B. Cantilever Vibration Modeling

Cantilever oscillation in an under damped system can be described using Newton's 2nd Law of motion where all internal and external forces acting on the cantilever are balanced. Often times in cantilever vibration analysis, the inertial, spring and damping parameters are "lumped" and the resulting system is analyzed as a discrete-parameter system. In this research, however, the beam was modeled as a distributed-parameter or continuous system in one dimension to better account for inertial, elastic and dissipative effects during PA excitations. This approach also made it possible to directly compare analytic and finite element methods (FEM) modeling results of modal effects for the transversely loaded beam. Of particular interest was the case of forced motion with low damping where decreased damping and lowered resonance resulted in the highest deflection for a given applied force.

Cantilever natural vibration frequencies are important considerations when designing highly sensitive devices for low pressure environments. A simple equation for the natural frequencies of an undamped, uniform beam with a fixed end and a free end is

$$f_i = \frac{\beta_i^2}{2\pi}\sqrt{\frac{gEI}{l^4 w}} \quad (6)$$

where β_{i} is the boundary condition dependent i^{th} root of the frequency equation (Fundamental Mode; $\beta_1 = 1.875$ and Second Mode; $\beta_2 = 4.695$), g is the gravitational constant, E is Young's modulus, I is the moment of inertia, l is the length and w is the width of the beam.[22]

Using Equation 5 low pressure photoacoustic conditions, experienced by the cantilever, were predicted and used as load values for FEM modeling and simulation to evaluate a variety of beam designs. In an earlier work, the authors' used the CoventorWare FEM software suite to predict cantilever modal responses. The results showed that increased width to length ratio beams exhibited decreased second harmonic torsional mode frequency and higher sensitivity.[23] Based on this result, harmonic pressure loads as a function of frequency were applied to the top surface of the cantilever to find maximum tip deflection. A mass-proportional cantilever damping parameter, defined as a fraction of the critical damping coefficient ($C_{m-p} = \lambda C_0$), was also used during the simulations.[24] The damping conditions were set ($\lambda = 0.1$ %) to simulate a low pressure environment necessary for THz PA testing. Simulated sinusoidal load pressures of 0.03-7.5 μ Torr resulted in amplitude displacements of 0.14-2.8 μ m, respectively. These results, based on realistic estimates of PA pressures, predict cantilever deflections that can be reliably measured using laser interferometer.

Further analysis of the analytic and FEM results highlights two key factors that were considered prior to device fabrication: 1) the magnitude of the tip displacement and 2) the cantilever's resonant frequency. If the PA system is modulated at the cantilever's resonant frequency, a higher beam resonance enables a greater number of signal averages over a shorter data collection period. Equation 5, however, suggests that using a low resonant frequency beam is beneficial because the change in chamber pressure per cycle is inversely proportional to system modulation frequency. Low-k, mm-size cantilevers with low resonant frequencies are difficult to fabricate due to their large size and fragile nature. Based on these considerations, $5 \times 2 \times 0.01\text{mm}^3$ (*length x width x thickness*) cantilevers with predicted resonant frequencies of approximately 626 Hz were fabricated.

C. Fabrication and Experimental Setup

Large surface area cantilevers, with high length to thickness ratios (500), were designed for maximum sensitivity. The beams were fabricated using Ultrasil silicon-on-insulator (SOI) (100) wafers. First a reflective layer of Ti/Au (20/100 nm) was evaporated at the end of the beam to allow in-situ interferometer measurements during PA testing. A Plasma-Therm Versaline deep reactive ion etch (DRIE) system was used to etch 3-8 μ m gaps in the SOI device layer to define the planform of cantilever. The main advantage of using an anisotropic DRIE etch was cantilever near vertical sidewalls and minimized undercutting of the masking layer. The SOI handle wafer, under the beam, was removed using a two step DRIE/RIE etching process until the etch stop silicon dioxide layer was reached.[23] Due to the high length to thickness ratio, however, the backside etch process proved challenging. The brittle nature of the mm-sized silicon beams and the residual stresses between the device and buried oxide (BOX) layers caused highly localized stress points resulting in cracks in early fabrication attempts. These fabrication challenges were overcome by using a photoresist support layer and a thinner SOI BOX layer to lower residual stress and increase manufacturability. The cantilevers were released using a hydrofluoric acid vapor etch to remove the BOX layer and then tested in a custom-built vacuum chamber.

The THz PA test chamber, constructed from stainless steel, has a volume of approximately 8 in^3 and consists of two segments. The back segment contains the absorption cell while the front portion contains a small balance volume. The chamber's absorption region was a 2 in long cylinder that was 10 mm in diameter. A system photograph and exploded view diagram of the vacuum chamber, including cantilever position, is shown in Fig. 2.

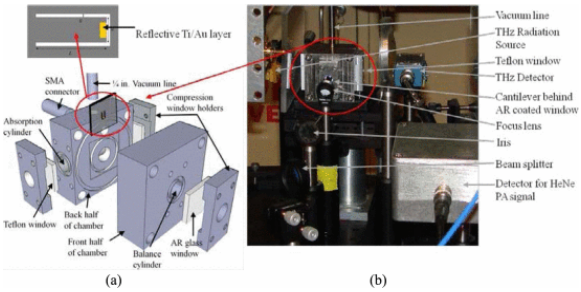

Fig. 2. (a) Exploded view schematic diagram of the photoacoustic (PA) test cell including a top view of the cantilever. (b) Photograph of the entire assembled THz PA system.

Liquid methyl cyanide (CH_3CN) was introduced into the vacuum chamber through a series of valves. The vaporized CH_3CN was then metered into the acoustic cell while the absolute chamber pressure was continuously monitored using an MKS Baratron® vacuum gauge. Data collections were monitored and controlled using LabVIEW and spectral data were collected using a National Instruments (NI) USB-6221 multifunction data acquisition card. A Virginia Diodes Inc. (VDI) source, controlled by an Agilent E8254A PSG-A signal generator, was used to generate 0.6–1.4 mW radiation from 0.250-0.375 THz. At low chamber pressures, the THz source power was attenuated to prevent molecular saturation. At the opposite side of the vacuum chamber a detector was positioned to monitor THz radiation exiting the chamber. The PA chamber and optics for the experiment were assembled on an optical bench as illustrated in Fig. 3.

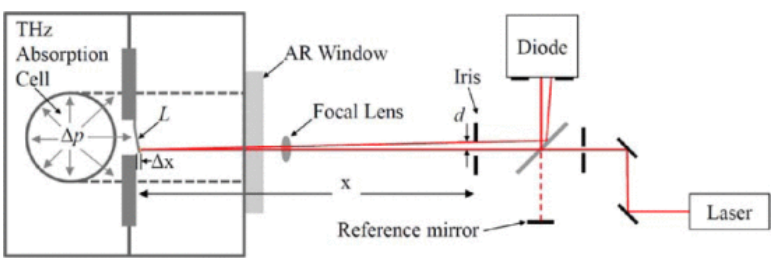

Fig. 3. Diagram (not to scale) showing both photoacoustic optical measurement techniques: 1) iris beam clipping; and 2) Michelson interferometer.[25]

An iris beam clipping or optical beam deflection method, similar to Garcia-Valenzuela *et al*. was used to collect THz PA spectral data from the test chamber.[25] To quantify the sinusoidal changes in power observed at the photodiode, a Michelson interferometer measurement was also incorporated into the experimental setup. In both measurements (clipped beam and Michelson interferometer), the VDI signal was sent to a Stanford Research Systems SR560 preamplifier and a SR530 lock-in amplifier. The VDI's amplitude modulated frequency input, from the signal generator, was also used as the reference signal for the lock-in amplifier.

D. Results and Analysis

Methyl cyanide was selected as the test species in this study because of its well documented strong and weak absorption lines between 0.018–1.8065 THz. Initial PA data were collected at an absorption line of approximately 312.63 GHz and a system modulation frequency scan from 1-700 Hz. The data, graphed in Fig. 4, shows that optimal PA signal resulted when the system modulation frequency was matched to

the cantilever's resonant frequency ($\omega \cong \omega_o$) as predicted by simulation. The data also shows a slight increase in modulation frequency with increased pressure, as well as, increased PA signal with higher chamber pressures which corresponds to a lowered signal quality factor. Each of these findings will now be discussed.

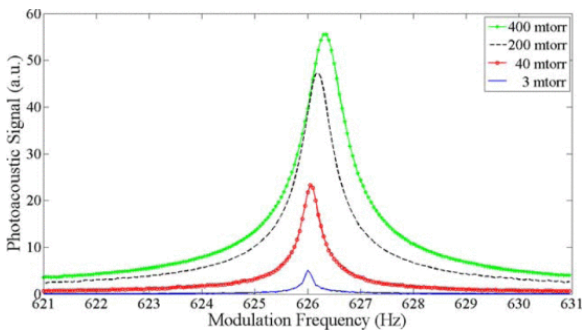

Fig. 4. Photoacoustic (PA) response of the cantilever, as a function of modulation frequency, for four different chamber pressures shows that optimal PA signal resulted when system modulation frequency was equal to the cantilever resonant frequency ($\omega \cong \omega_o$) as was predicted by simulation. The data also shows a slight increase in modulation frequency with increased pressure, as well as, increased signal with decreased signal quality factor.

The required modulation frequency to achieve the maximum PA signal peaks increased non-linearly with increasing chamber pressure by approximately 8.8×10^{-4} Hz/mTorr over all. The blueshift in frequency was due to an increased effective spring constant related to gas interaction with the cantilever that increased as a function of chamber pressure.20 More importantly, from the modulation frequency scan data, the quality factor of the cantilever decreased with increased chamber pressure. This is a critical result and a necessary consideration for high spectral resolution measurements. The quality factor of a cantilever can be expressed as

$$Q = \frac{\omega_o}{\Delta\omega} = \frac{f_o}{\Delta f} \quad (7)$$

where f_o is the fundamental frequency of the cantilever and Δf is the full width half maximum of the PA signal. Due to the low damping conditions of the rarified gas in the PA chamber, the cantilever had sharp resonant responses to the modulation frequency scans with corresponding small Δf values (0.15-1 Hz). At low pressures, the $5 \times 2 \times 0.01$ mm^3 cantilever exhibited very high quality factors shown in Fig. 5. The impacts of this finding on the spectral resolution will be addressed later.

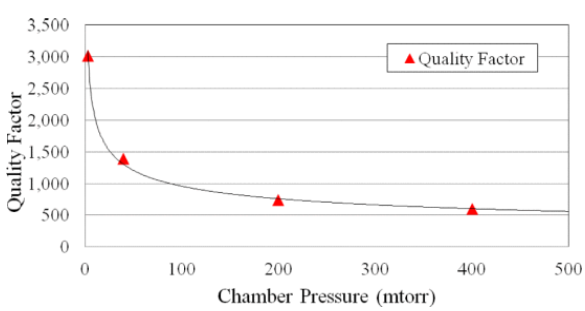

Fig. 5. Quality factor variation of a $5 \times 2 \times 0.01$mm^3 cantilever as the chamber pressure increases. The data shows very high Q at low chamber pressures due to the low pressure intrinsic/molecular damped environments in the photoacoustic chamber.

Utilizing the optimal modulation frequency at each pressure, the dynamics of cantilever excitation and relaxation were investigated next. Shown in Fig. 6. is a sample of PA data collected at a chamber pressure of approximately 3 mTorr. The data shows a THz excitation time of approximately 9 sec and the PA lock-in signal approaching steady state just prior to the THz radiation being turned off. As the chamber pressure was increased, the PA signal response time improved.

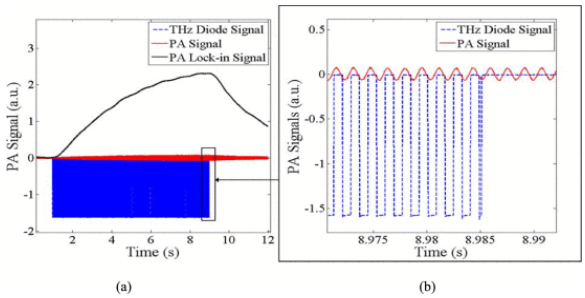

Fig. 6. Photoacoustic (PA) data recorded at 3 mTorr in plot (a) shows the slow response of the lock-in amplifier and raw PA signals at the low chamber pressure. Plot (b) is a zoomed in view of the raw PA signal from the diode and modulated THz signal as the radiation is turned off.

Fig. 7 is a sample of PA data collected at a chamber pressure of 80 mTorr with a similar excitation time of approximately 9 sec. The higher chamber pressure showed a quicker response and steady state conditions being achieved in approximately 4 sec.

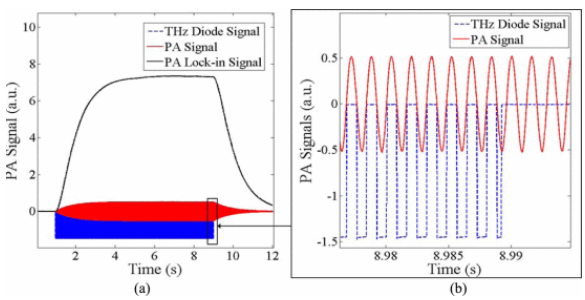

Fig. 7. Photoacoustic (PA) data in plot (a), taken at 80 mTorr, illustrates the quicker response time of the lock-in PA signal and raw PA signal from the THz excitation radiation at higher chamber pressure. Plot (b) is a zoomed in view of the raw PA signal from the diode and modulated THz signal.

For a range of pressures, the cantilever was excited to steady state conditions and then the THz signal was turned off with the decaying PA signal recorded. An exponential curve fit was used to extract the decay time constant. The resulting time constant verses pressure plot is shown in Fig. 8. The time constant data shows increased decay time constant with decreased chamber pressure as the environment transitions from the molecular to the intrinsic pressure regime. At a chamber pressure of approximately 3 mTorr, the PA signal decayed to steady state in approximately 8 seconds. The long excitation and decay times, at lower chamber pressures, were expected due to the extremely low pressure change (μ Torr range) that was generated during each THz modulation pulse.

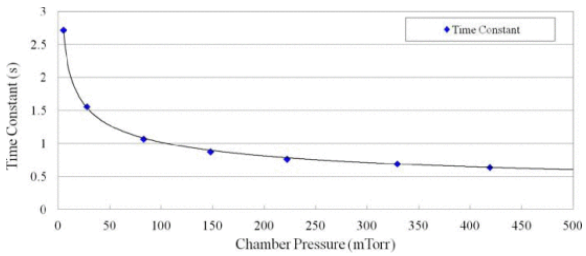

Fig. 8. Time constants found through exponential curve fit to the decay of photoacoustic signals over the range of pressures shown.

To further quantify the PA signal being generated, cantilever displacement measurements were collected using the Michelson interferometer configuration previously discussed. Peak-to-peak PA signal and cantilever tip displacement measurements are compared in Fig. 9.

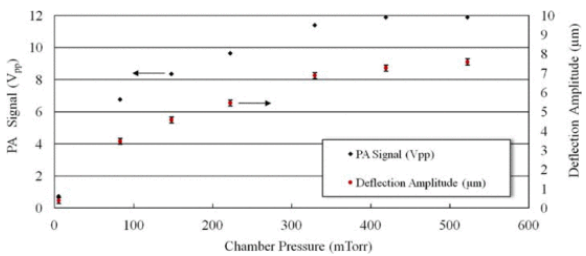

Fig. 9. Graph of measurements taken on $5 \times 2 \times 0.01\text{mm}^3$ cantilever at different chamber pressures shows highly correlated photoacoustic peak-to-peak signals and interferometrically measured cantilever amplitude deflections.

The data shows that extremely low chamber pressure conditions (< 0.1 mTorr) resulted in minimal PA signal be measured. The graph also shows that chamber pressure increases with the addition of methyl cyanide gas and that PA signal and cantilever deflection also increase linearly and are well correlated. Above approximately 7 μ m of cantilever deflection, the PA signal increases only slightly due to the positioning of the laser beam through the iris. The strong correlation between PA signal and beam deflection justifies using the iris clipped method based on intended chamber pressures (2-40 mTorr) and the resulting range of cantilever deflection. Another advantage of this method is that modest sampling rates allow for multiple data channels.

The noise content of the collected PA data was investigated next. In Fig. 10, a 1 sec duration data set was evaluated using Fourier analysis. The data shown in the Fig. 10 is a single-sided amplitude FFT with the THz source turned off. With the THz source operating at 312.63 GHz (modulation frequency of 626.02 Hz), the system exhibited a very high SNR. The noise content that was observed, however, was attributed to the experiment not being vibration isolated on an optical bench and to other equipment being operating in the laboratory.

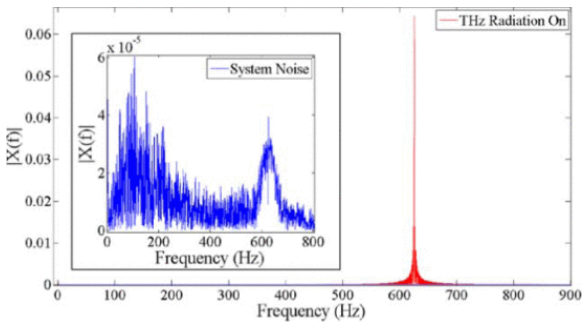

Fig. 10. Fourier analysis of a one sec photoacoustic (PA) signal, collected at 200 mTorr taken at 312.63 GHz, showed low noise in the system using the iris clipped PA measurement method.

Photoacoustic spectral data collection was also performed across a range of pressures. As discussed earlier, chamber pressure greatly affects PA signal strength and cantilever response time. Therefore, two data collection techniques were investigated; a fast scan method to quickly measure a broad frequency spectrum and a slow scan method to obtain higher quality PA spectral data in a narrow passband. PA measurements were collected in two steps or intervals: 1) beam excitation time and 2) signal averaging period. The first interval was the time needed to reach optimum beam amplitude displacement and the second interval was time period used for signal averaging. The data measured during the signal averaging period was recorded for each THz frequency prior to the frequency being incremented and the measurement sequence repeated.

The effect of excitation time was investigated with the signal averaging period held constant (0.1 sec) for each of the trials. Fig. 11. shows the results of three excitation times taken at a chamber pressure of 59 mTorr with a frequency step size of 0.05 MHz. The 2 sec excitation time data collection took 9.7 min, the 0.5 sec excitation time took 2.8 min, and the 0.1 sec excitation time took 0.9 min to collect. The PA response shows a noticeable blueshift in frequency, a reduction in signal strength as excitation time decreases and noticeable peak broadening as discussed earlier.

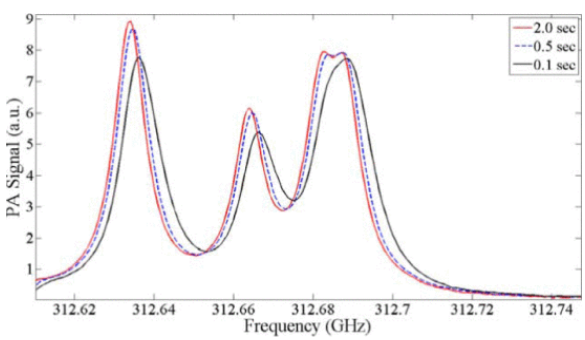

Fig. 11. Spectral PA signals taken at 59 mTorr with 2, 0.5, and 0.1 sec excitation times using a 0.05 MHz step size, moving from low to high frequency, the PA peak response shifted to higher frequencies and reduced amplitudes as the excitation time was decreased.

During the low pressure (2-40 mTorr) PA data collections, the rising edge of the signal takes between 4-12 sec due to the low excitation pressures generated in the chamber and the high quality factor of the cantilever. Likewise, the falling edge also transitions slowly as the cantilever reaches steady state, due to the small damping coefficient at the lower chamber pressures and the continued excitation at lower absorption strengths.

To achieve highly accurate absorption frequencies during spectral scans, the excitation time was increased as the chamber pressure was decreased. At lower chamber pressures (2-5 mTorr), spectral line broadening was only due to Doppler broadening resulting in narrow spectral lines. As line broadening increased with pressure, the frequency step size was increased and the excitation time decreased. In Fig. 12, PA spectra were recorded for three low pressure cases. Each collection took 10-12 hours due to the small 0.05 MHz step size and the 12-15 sec excitation time needed before subsequent 0.5 sec average signals were recorded. The resulting PA spectra contain strong absorption lines at higher chamber pressure while lower chamber pressures reveal previously obscured absorption lines. For example, at 40 mTorr the 312.7 GHz absorption peak has higher signal but obscures two lower peaks that are separated by only 6 MHz. At lower chamber pressures (2 mTorr and 16 mTorr), the spectral resolution is much improved due the higher Q at the lower pressures.

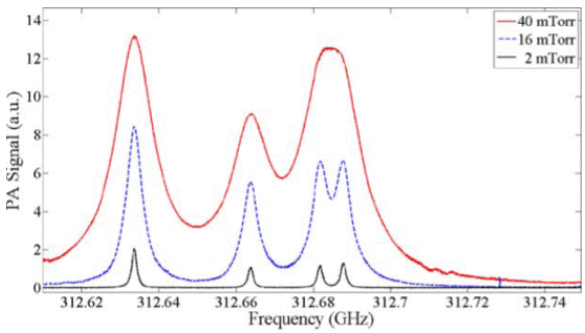

Fig. 12. Photoacoustic (PA) spectral data of CH_2CN collected at three pressures used utilized a 0.05 MHz step size and recorded the 0.5 sec average PA signal for each frequency step.

To demonstrate the spectral performance of this novel THz PA system, a 1.07 GHz frequency scan was performed at 13 mTorr and spanned 311.72-312.79 GHz. This low pressure PA data, shown in Fig. 13, successfully captured 13 methyl cyanide absorption lines using a 0.2 MHz step size, a 12 sec excitation time and a 0.5 sec averaged signal. This wider bandwidth scan took approximately 12.5 hrs to collect and was plotted along with a simultaneously recorded THz diode signal and the previously modeled absorption coefficient (Fig. 1). The simulated spectra very closely matches the measured data with small deviations noted at the higher absorption strengths.

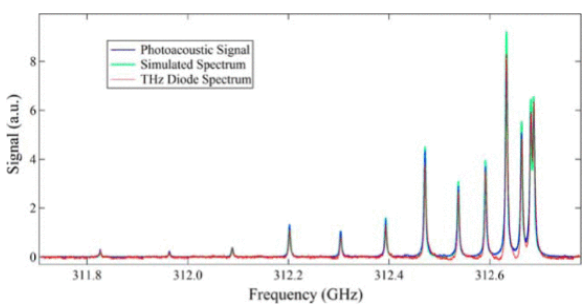

Fig. 13. Photoacoustic data and the simultaneously recorded THz diode signal are compared to the simulated absorption spectra of methyl cyanide recorded at 13 mTorr of chamber pressure.

Once repeatable high quality PA data collections were demonstrated; overall system performance was evaluated and compared to other THz PA systems found in the literature. As previously discussed; SNR, system sensitivity and NNEA are important FOM parameters for comparing system performance. The data collected at 13 mTorr is representative of the low chamber pressure data collected during

throughout this study and shows a highly resolved PA absorption peak (7.08 au) at 312.6336 GHz. The RMS noise floor for this data set was approximately 0.0058 resulting in a SNR of 1,221. Using Equations (1) and (2), system sensitivity and NNEA were calculated using a 0.5 sec signal averaging time. The resulting system sensitivity ($1.97 \times 10^{-5}\ \mathrm{cm}^{-1}$) and NNEA ($1.39 \times 10^{-9}\,\mathrm{cm}^{-1}$ W $\mathrm{Hz}^{-1/2}$ compared very well to other PA systems reported in the literature.[5–6,7,8,9,10,11,12,13,14,15,16,17,18,19,20] The contributions of this research include demonstrating a compact THz PA system at very low chamber pressures (2-40 mTorr) resulting in extremely high Q values (~2500) with exceptional spectral resolution (~6 MHz).

SECTION II. Conclusions

THz radiation and the corresponding PA response are useful parameters for identifying chemical agents in hazardous environments. In this study, a MEMS cantilever was successfully modeled, fabricated, tested and integrated into a custom-built, compact, low vacuum, THz PA chemical sensing and molecular spectroscopy system. Cantilever design parameters of length, width and thickness were successfully used to design a device capable of sensing extremely low PA pressures. Despite a difficult (albeit straightforward) fabrication process, due to high length to thickness beam ratios, a novel, first-ever MEMS cantilever-based THz photoacoustic spectrum was collected and analyzed at very low chamber pressures (2-40 mTorr). The pressure regimes tested were several orders of magnitude lower than non-THz-based, PA trace gas detection systems.[11–12,13,14,15,16,17,18] This low pressure (high Q) environment resulted in high SNR PA signals with excellent spectral resolution at chamber pressures as low as 2 mTorr. The sensor size and chamber pressures presented here were also an order of magnitude smaller than those presented by the closest comparable THz PA system [9]. Additionally, a fast “coarse” scan technique to rapidly evaluate small spectral regions and a slow “fine” scan technique to accurately measure highly resolved absorption frequencies were developed. Based on the results and the scan techniques developed, a semi-portable, “leave on the battlefield” chemical agent sensing device is now possible and could eventually lead to a fully portable or hand-held chemical sensing system.

ACKNOWLEDGEMENTS

The authors would like to thank the Air Force Research Laboratory (AFRL) Sensors Directorate for assisting with fabrication. The authors would also like to thank AFIT’s cleanroom staff, Mr. Richard Johnston and Mr. Thomas Stevenson.

References

1. A. G. Bell, Upon the Production of Sound by Radiant Energy, Washington, DC, USA:Gibson Brothers, Printers, 1881.

2. G. A. West, J. J. Barrett, D. R. Siebert, K. V. Reddy, "Photoacoustic spectroscopy", *Rev. Sci. Instrum.*, vol. 54, no. 7, pp. 797-817, 1983.

3. A. Miklós, P. Hess, Z. Bozóki, "Application of acoustic resonators in photoacoustic trace gas analysis and metrology", *Rev. Sci. Instrum.*, vol. 72, no. 4, pp. 1937-1955, 2001.

4. W. Brugel, An Introduction to Infrared Spectroscopy, Hoboken, NJ, USA:Wiley, 1962.

5. A. A. Kosterev, Y. A. Bakhirkin, R. F. Curl, F. K. Tittel, "Quartz-enhanced photoacoustic spectroscopy", *Opt. Lett.*, vol. 27, no. 21, pp. 1902-1904, Nov. 2002.

6. A. A. Kosterev, F. K. Tittel, D. V. Serebryakov, A. L. Malinovsky, I. V. Morozov, "Applications of quartz tuning forks in spectroscopic gas sensing", *Rev. Sci. Instrum.*, vol. 76, no. 4, 2005.

7. K. Liu et al., "Trace gas sensor based on quartz tuning fork enhanced laser photoacoustic spectroscopy", *Appl. Phys. B Lasers Opt.*, vol. 94, no. 3, pp. 527-533, 2009.

8. S. Borri et al., "Terahertz quartz enhanced photo-acoustic sensor", *Appl. Phys. Lett.*, vol. 103, no. 2, pp. 021105, 2013.

9. A. F. Krupnov, A. V. Burenin, K. N. Rao, "New methods in submillimeter microwave spectroscopy", *Molecular Spectroscopy: Modern Research*, pp. 93-126, 1976.

10. S. L. Firebaugh, K. F. Jensen, M. A. Schmidt, "Miniaturization and integration of photoacoustic detection with a microfabricated chemical reactor system", *J. Microelectromech. Syst.*, vol. 10, no. 2, pp. 232-237, Jun. 2001.

11. N. Ledermann, P. Muralt, J. Baborowski, M. Forster, J. Pellaux, " Piezoelectric Pb(Zr x Ti 1− x)O 3 thin film cantilever and bridge acoustic sensors for miniaturized photoacoustic gas detectors ", *J. Micromech. Microeng.*, vol. 14, no. 12, pp. 1650-1658, 2004.

12. T. Kuusela, J. Peura, B. A. Matveev, M. A. Remennyy, N. M. Stus', "Photoacoustic gas detection using a cantilever microphone and III–V mid-IR LEDs", *Vibrat. Spectrosc.*, vol. 51, no. 2, pp. 289-293, Nov. 2009.

13. T. Kuusela, J. Kauppinen, "Photoacoustic gas analysis using interferometric cantilever microphone", *Appl. Spectrosc. Rev.*, vol. 42, no. 5, pp. 443-474, Sep. 2007.

14. E. D. McNaghten, K. A. Grant, A. M. Parkes, P. A. Martin, "Simultaneous detection of trace gases using multiplexed tunable diode lasers and a photoacoustic cell containing a cantilever microphone", *Appl. Phys. B Lasers Opt.*, vol. 107, no. 3, pp. 861-871, 2012.

15. B. D. Adamson, J. E. Sader, E. J. Bieske, "Photoacoustic detection of gases using microcantilevers", *J. Appl. Phys.*, vol. 106, no. 11, pp. 114510, 2009.

16. J. Fonsen, V. Koskinen, K. Roth, J. Kauppinen, "Dual cantilever enhanced photoacoustic detector with pulsed broadband IR-source", *Vibrat. Spectrosc.*, vol. 50, no. 2, pp. 214-217, 2009.

17. J. Peltola et al., "High sensitivity trace gas detection by cantilever-enhanced photoacoustic spectroscopy using a mid-infrared continuous-wave optical parametric oscillator", *Opt. Exp.*, vol. 21, no. 8, pp. 10240-10250, 2013.

18. J. Kauppinen, K. Wilcken, I. Kauppinen, V. Koskinen, "High sensitivity in gas analysis with photoacoustic detection", *Microchem. J.*, vol. 76, no. 1, pp. 151-159, 2004.

19. P. Sievilä, N. Chekurov, J. Raittila, I. Tittonen, "Sensitivity-improved silicon cantilever microphone for acousto-optical detection", *Sens. Actuators A Phys.*, vol. 190, no. 1, pp. 90-95, 2013.

20. V. Koskinen, J. Fonsen, K. Roth, J. Kauppinen, "Progress in cantilever enhanced photoacoustic spectroscopy", *Vibrat. Spectrosc.*, vol. 48, no. 1, pp. 16-21, 2008.

21. F. R. Blom, S. Bouwstra, M. Elwenspoek, J. H. J. Fluitman, "Dependence of the quality factor of micromachined silicon beam resonators on pressure and geometry", *J. Vac. Sci. Technol. B Microelectron.*, vol. 10, no. 1, pp. 19-26, 1992.

22. W. T. Thomson, Theory of Vibration with Applications, Englewood Cliffs, NJ, USA:Prentice-Hall, 1972.

23. N. E. Glauvitz, R. A. Coutu, M. Kistler, I. R. Medvedev, D. T. Petkie, "MEMS cantilever sensor for photoacoustic detection of terahertz radiation", *Proc. SEM Annu. Conf. Exposit. Experim. Appl. Mech.*, pp. 1-6, 2013.

24. J. J. Thomsen, Vibrations and Stability, Berlin, Germany:Springer-Verlag, 2003.

25. A. Garciá-Valenzuela, J. Villatoro, "Noise in optical measurements of cantilever deflections", *J. Appl. Phys.*, vol. 84, no. 1, pp. 58-63, 1998.